EUROPEAN ORGANIZATION FOR NUCLEAR RESEARCH

CERN-PPE/93-140
23 June 93
CERN-LAA/SF/93-06

PHOTONCOUNTING WITH A HYBRID PHOTOMULTIPLIER TUBE (HPMT)*

C. D'Ambrosio, T. Gys, H. Leutz, D. Piedigrossi, D. Puertolas and S. Tailhardat
CERN, Geneva, Switzerland

Abstract

In comparison with a photomultiplier tube, the resolving power for photoelectron peaks is largely improved by a silicon diode bombarded with electrons from a light detecting photocathode. With photoelectrons accelerated to 13 keV, the measured variance of the electronic noise is 1.29 keV and the total variance of the photoelectron peaks is 1.81 keV. The continuum part of the photoelectron spectrum is explained by a backscattering process on the diode surface. The contrast function shows that up to 14 photoelectron peaks can be resolved.

To be submitted to Nucl. Instr. and Methods

* The work reported here is part of the LAA - Project

1. INTRODUCTION

Counting of photons emitted from weak light sources becomes more and more important in physics and astronomy. To achieve reliable results for the emission of single and multiple photoelectrons, arising from light absorption in a photocathode, it is of utmost importance to resolve their associated counting peaks. Therefore, many experimental procedures have been applied to improve the energy resolution of photoelectron peaks. Most of them are based on photomultipliers, in particular on the Quantacons * with a cesiated gallium-phosphide first dynode, which provides increased emission of secondary electrons. The statistical fluctuations of the electron multiplication at this first dynode is responsible for the intrinsic energy resolution. Due to the high gain of photomultipliers, the contribution of the electronic amplifiers can be neglected.

With a Quantacon we could only resolve up to three photoelectron peaks [1]. Therefore we decided to apply a silicon diode, which is bombarded with electrons from a light detecting photocathode. The principle of such devices is well known [2], and has been further developed by R. DeSalvo [3]**. An electrostatically focused type is now commercially *** available. Each photoelectron hitting the silicon diode creates some 275 electron-hole pairs per keV electron energy within its depleted volume. Accelerating the photoelectrons to 13 keV by the corresponding potential difference between photocathode and silicon diode, results in some 3500 electron-hole pairs. This number is by more than two orders of magnitude higher than the yield at the first dynode of a photomultiplier and hence the statistical fluctuations are considerably smaller. In contrast to the photomultiplier however, the total gain of a silicon diode is by more than two orders of magnitudes smaller and therefore the noise contribution of the connected preamplifier contributes accordingly to the energy resolution of the photopeaks.

This paper reports on first experiences and results we obtained with a hybrid tube containing a silicon diode and a photocathode (HPMT). In particular, we describe contributions from electron backscattering from the diode, random signals from the light emitting source, thermal electron emissions from the photocathode, and capacitive noise from the subsequent electronic components. Moreover, after successful tests, we intend to apply similar devices for the detection of light signals from small diameter (60 μm) scintillating fibres. For this purpose, the single diode would be replaced by an array of small silicon pixels and the electrostatic focussing by a magnetic (or proximity) one.

---

* 8850, Burle Electron Tubes, Lancaster, PA, USA

** Recently, first test results have been reported on prototypes of proximity focussed devices [3b]

*** BV Delft Electronische Producten (DEP), NL-9300 AB Roden, The Netherlands

2. EXPERIMENTAL PROCEDURE

The photon detector is composed of the light detecting photocathode and the fully depleted silicon diode. Both are enclosed opposite to each other (fig.1) in a common vacuum tube. An electrostatic focussing system guides the photoelectrons, which are accelerated by a corresponding potential difference, from the cathode (18 mm diameter) onto the diode surface of 2 mm diameter. There, they cross a 0.1 μm insensitive n^+-contact layer before being absorbed within 2.5 μm of the 300 μm depletion layer. The charge signals of the silicon diodes are transmitted to the low noise preamplifier * outside the vacuum tube and are further processed according to the bloc diagramme shown in fig.2.

The photons arise from a fused bundle of polystyrene scintillating fibres [4] of 2 m length with square cross-sections of 2.5 mm edges containing about 1600 individual fibres of hexagonal shape **. The scintillating light of this bundle was excited with β^--particles from a Sr-90 (37 MBq) source. A common support (fig.3) positioned this β-source underneath and the two coincidence detectors above a 2.5 m long bench, which contained the fibre bundle in its longitudinal groove.The coincidence counters could be slid together with the β-source along the bench into the wanted fibre positions. The photons reaching one end of the bundle and the photocathode were transformed into photoelectrons, and accelerated onto the silicon diode. Its charge signals were gated with electronic pulses from the coincidence counters according to fig.2. The average number of detected photoelectrons could be changed by varying the source position along the fibre bundle and, in addition, introducing grey filters at the extreme source position of 2 m distance in order to further reduce this number. The photoelectron spectrum was finally recorded via an ADC*** or a multichannel analyser**** with a PC.

3. MEASUREMENTS AND RESULTS

To examine the composition of the energy resolution for the expected photoelectron peaks we first investigated the electronic noise which manifests itself in the variance σ_{ped} of the pedestal. For this purpose we replaced the HPMT at the preamplifier input with capacitors of different values and measured σ_{ped} as function of the capacitance (fig.4). After that, we reconnected the HPMT again to the preamplifier and measured σ_{ped} with

---

* Model 142A, ORTEC, Oak Ridge, TN, USA
** KURARAY Co, Ltd. Methacrylic Resin Division, Tokyo 140, Japan
*** ADC Camac Module 2259, Le Croy, Meyrin, Switzerland
**** Silena Multichannel Analyser (mod. 7423 VHS), SILENA, Cernusco, Italy

150 V bias across the depleted diode layer, but at zero potential difference between photocathode and diode. The measured value is marked in fig.4 and would correspond to a measured equivalent input capacitance of 16 pF.

Then, we determined the capacitances of the HPMT at different bias voltages (fig.5), again with zero potential difference. Between 40 V and 150 V bias its average capacity amounts to 15 pF, in good agreement with that deduced from σ_{ped} = 1.16 keV (16 pF) in fig.4 and with the total of 12 pF measured for the individual components of the HPMT set-up listed in fig.5. Applying 13 kV potential difference we measure σ_{ped} = 1.29 keV (fig.6) which we shall call now the electronic variance $\sigma_{electr.}$ namely the electronic noise contribution to the variance of the photoelectron peaks. The increase of 0.13 keV is due to some 2 pF stray capacity activated inside the HPMT by the applied potential difference.

The tail of the pedestal in fig.6 and the parasitic peak, which corresponds to one photoelectron, arise from two sources : thermally emitted electrons from the photocathode (dark current) and random signals falling accidentally into the gate (fig.2). The random signals are uncorrelated photons induced by those electrons of the ß-source in the fibre bundle, which do not release a signal in the coincidence photomultipliers.

In order to further optimize the operating conditions of the HPMT, we measured the peak-to-valley ratios and the channel distances between the photoelectrons as a function of the applied bias voltage. Both curves in fig.7 show similar shapes, a sharp rise followed by a plateau starting at around 40 V bias and extending over 200 V. In a similar way, we measured the same parameters at different potential differences between photocathode and diode with the depletion bias fixed at 150 V. The results show in fig.8 a linear rise for both parameters. The resolution of individual photoelectron peaks disappears at around 5 kV. A plateau cannot be obtained, since it should only appear at electron energies, where the corresponding range in silicon exceeds the 300 µm thickness of the depleted diode layer (~250 keV). This potential difference (250 kV) is by far beyond the tolerable value (15 kV) indicated by the manufacturer, for the HPMT.

Typical photoelectron spectra are displayed in figs 9 and 10 for an average $<n>_{meas}$ of 1.3 and 5.4 photoelectrons resp., where

$$<n>_{meas} = \frac{\sum_m q_m N_m}{\sum_m N_m} \qquad (1)$$

and q_m is the channel number in photoelectron units (see figs 9 and 10), N_m is the number of counts per channel (see also [1]). Fig.9 indicates the definition of peak, valley, and Δ channel values used for figs 7 and 8. Both figures display also the variances with statistical errors for the photoelectron peaks.

4. DISCUSSION

The spectra displayed in figs 9 and 10 are composed of discrete gaussian shaped peaks, each associated with an integer number m of photoelectrons, and of a continuum. The variances σ_m increase from (1.29 ± 0.04) keV for the pedestal to an average of (1.81 ± 0.08) keV (fig.10) for the peaks with $m \geq 1$. This behaviour follows the relation :

$$\sigma^2_{total} = \sigma^2_{electr.} + \sigma^2_{diode} \tag{2}$$

which results in $\sigma_{diode} = (1.27 \pm 0.07)$ keV due to the fluctuations of the electron-hole pair number.

The peaks in figs 9 and 10 can be simulated from relation (2) and the Poisson distribution:

$$P_m(< n >) = \frac{< n >^m}{m!}\ e^{-<n>} \tag{3}$$

with $<n> = \text{const } <E>$ meaning the average number of photoelectrons resulting from the average energy loss $<E> = 500$ keV of a minimum ionizing particle passing through the 2.5 mm of the fibre bundle.

This Poisson distribution (3) must be supplemented by the Landau (Vavilov) distribution [5] with its most probable energy loss $E_p = 430$ keV again for a minimum ionizing particle passing through 2.5 mm of polystyrene. Therefore, relation (3) changes into :

$$P^L_m(< n >) = P^L_m(< E >) = \int_0^\infty L(E - < E >)\ P_m(E)\ dE \tag{4}$$

where E is the integration variable. Fig.11 shows the photoelectron peaks with their gaussian shapes simulated from relation (2) and their relative intensities simulated with relation (4) for $<n> = 6.2$.

Obviously, the continua in the spectral distribution of figs 9 and 10 cannot be explained by overlaps of the photoelectron peaks, if we compare fig.10 with fig.11. Therefore, we are obliged to consider other processes, in particular the backscattering of the accelerated photoelectrons from the diode surface. The backscattered fraction $\alpha = 0.18$ [6] of 13 keV electrons deposit on average half of their 13 keV energy within the sensitive diode volume. To take this backscattering process into account, we simulate a distribution of the absorbed photoelectron energies q. The probability is $B_1(q_1) = (1-\alpha)$ if the photoelectron is completely absorbed, and it is uniform between 0 and q_1 (and equal to α/q_1) in case of backscattering. This probability distribution can be extended to m photoelectrons by the relation

$$B_m(q) = \int_0^{q_m} B_{m-1}(q')\ B_1(q-q')\ dq' \qquad (5)$$

with the normalization: $\int_0^{q_m} B_m(q')\ dq' = 1$.

Relation (5) must now be folded with the electronic noise showing up in the pedestal, and we obtain :

$$B'_m(q) = \int_0^{q_m} B_m(q')\ e^{-\frac{(q-q')^2}{2\sigma^2}}\ dq' \qquad (6)$$

As an example, the non backscattered intensities $B'_m(q_m) \propto (1-\alpha)^m$, are shown for m = 1, 2, 4, 6 and 9 together with the related backscattering intensities in fig. 12.

Finally, we take into account the Poisson and the Landau distribution (relation (4)) and are ready to simulate the following distributions :

$$\sum B'_m(q)\ P_m^L(< n >) \qquad (7)$$

which are displayed together with the measured ones for <n> = 1.5 and <n> = 6.2 in figs 13 and 14 resp.. The only parameters entering these simulations are the backscattering coefficient (including now the dark current contribution and that of accidental coincidences) $\alpha = 0.23$, the variance σ and the average number of photoelectrons <n> relative to the measurements we want to fit.

As the effect of backscattering is to decrease the average number of electron-hole pairs generated by a photoelectron, $<n>_{meas}$ from rel. (1) will be smaller than $<n>$ * :

$$< n >_{meas} \approx \; < n > \left(1 - \frac{\alpha}{2}\right) \tag{8}$$

The average contributions of the diode (1.27 keV) and of the electronic noise (1.3 keV) to the total variance of the photoelectron peaks (relation (2)) mask entirely the normally adopted intrinsic variance ($\sigma_{intr.}$), which adds to the variance ($\sigma_{electr.}$) of the pedestal :

$$\sigma^2_{intr} = m \; F \; E_0 \; \varepsilon \tag{9}$$

with $F \sim 0.1$ meaning the Fano factor, $E_0 = 13$ kV the acceleration potential of the photoelectrons, $\varepsilon = 3.65$ eV the expended energy to create one electron-hole pair, and m the number of photoelectrons released from the photocathode. This results in $\sigma_{intr.}(1) = 0.07$ keV and $\sigma_{intr.}(7) = 0.18$ keV for one or seven photoelectrons, resp.. This is still within the error margins listed in figs 9 and 10. Due to the dominant backscattering contribution, it is therefore impossible to identify the intrinsic diode contribution $\sigma_{intr.}$.

The number of photoelectron peaks resolved with the present HPMT is compared in fig.15 with that of a Quantacon. The better performance of the HPMT arises from higher electron statistics in the diode as compared to the rather poor electron multiplicity achieved with the first Quantacon dynode. The peak and valley values are taken from fig.4 in ref.[1] for the Quantacon and from fig.10 of this paper for the HPMT. Without backscattering, the contrast function of the HPMT would indicate some 100 resolved photoelectron peaks, provided a light source of corresponding intensity is applied. This resolving power is due to the small intrinsic variance of semiconductors which adds to the electronic noise.

---

* In fact, $<n>$ represents the average number of photoelectrons generated at the photocathode, while $<n>_{meas}$ is the average number of photoelectrons detected by the diode.

ACKNOWLEDGEMENTS

We wish to thank Prof. A. Zichichi for his continuous interest and generous support of our work. We also acknowledge substantial support from L. Boskma, DEP, Roden, The Netherlands and R. Bertin, CERN.

REFERENCES

[1] C. D'Ambrosio, T. Gys, H. Leutz, D. Puertolas, S. Tailhardat, T. Shimizu and O. Shinji, CERN-PPE/92-207, to be published in Nuclear Instruments and Methods in Physics Research

[2] F.S. Goulding, I.E.E.E. Transactions on Nuclear Science, June, (1964), 177.

R. Kalibjian, I.E.E.E. Transactions on Nuclear Science, August, (1965), 367.

J.M. Abraham, L.G. Wolfgang and C.N. Inskeep, Advances in Electronics and Electron Physics, (1966), 671.

J.M. Abraham, L.G. Wolfgang and C.N. Inskeep, I.E.E.E. Transactions on Nuclear Science, June, (1966), 46.

R. Kalibjian, I.E.E.E. Transactions on Nuclear Science, June, (1966), 54

P. Chevalier, Nuclear Instruments and Methods, 50, (1967), 346

J. Fertin, B. Lach, J. Meuleman, J. Dupuis, L. Hermite and R. Petit, I.E.E.E Transactions on Nuclear Science, NS-15, (1968), 179

E.A. Beaver, C.E. McIlwain, J.P. Choisser and W. Wysoczanski, Advances in Electronics and Electron Physics, 33B, 5th Symposium on Photoelectronic Image Devices, (1972), 863.

[3] R. DeSalvo, CLNS 87-92, Cornell University, Ithaca, 1987.

R. DeSalvo, W. Hao, K. You, Y. Wang and C. Xu, Nuclear Instruments and Methods in Physics Research, A315, (1992), 375.

[3b] H. Arnaudon et al., CERN-LAA/HC/93-16.

S. Basa et al., Nuclear Instruments and Methods in Physics Research, A330, (1993), 93.

[4] C. D'Ambrosio, H. Leutz, T. Shimizu and O. Shinji, Nuclear Instruments and Methods, A325, (1993), 161.

[5] U. Fano, Chairman of the Subcommittee on Penetration of Charged Particles. Publication 1133, (1964), 191 National Academy of Sciences-National Research Council, Washington, D.C.

[6] E.H. Darlington, J. Phys. D : Appl. Phys. 8 (1975) 85

FIGURE CAPTIONS

Fig. 1 The hybrid photo multiplier tube (HPMT)

Fig. 2 Bloc diagramme of the experimental arrangement

Fig. 3 Arrangement of β-source (1), fibre bundle (5) and coincidence counters with (7) meaning scintillator, (6) light guides, (9) PMT Hamamatsu R1635, (8) inactive plastic filter. (2) are collimator slits in plexiglas, (3) the common support structure for source and coincidence units, and (4) the bench guiding it and housing the fibre in its groove.

Fig. 4 Electronic noise (sigma) of the preamplifier for different input capacitances (measuring points and solid curve). Measured sigma with HPMT connected to the preamplifier (1.16 keV), which corresponds to 16 pF input capacitance.

Fig. 5 Dependance of HPMT capacitance from the silicon diode bias voltage. No potential difference between photocathode and diode.

Fig. 6 Measured electronic noise ($\sigma_{pedestal}$) with 150 V bias on diode and 13 kV potential difference. The tail arises from photocathode dark counts and from uncorrelated light signals falling randomly into the coincidence gate. Signals from coincidence photomultipliers (figs 2 and 3) are not connected.

Fig. 7 Peak-to-valley ratios and channel distances versus the bias voltage of the silicon diode. Plateaus are achieved from around 40 V bias extending over 200 V.

Fig. 8 Peak-to-valley ratios and channel distances versus the photoelectron acceleration voltage. The separation of the photoelectron peaks vanishes at around 5 kV potential difference. A plateau could only be expected at 250 kV where the photoelectron range exceeds the 300 μm thick depleted diode layer. This potential difference is far beyond the maximum tolerable value of 15 kV.

Fig. 9 Photoelectron spectrum for an average of 1.3 electrons. β-source distance 1.895 m and grey filter with 0.4 transmission between fibre bundle and photocathode (fig.2).

Fig. 10 Photoelectron spectrum for an average of 5.4 electrons. β source distance 1.295 m (fig.2).

Fig. 11 Photoelectron peaks simulated from relation (2) with their relative intensities simulated according to the Poisson- and Landau- distributions of relation (4).

Fig. 12 Examples for the simulated energy depositions and the backscattered intensities for different photopeaks.

Fig. 13 Measured photoelectron spectrum of fig.9 and the simulated one according to relation (7) (dashed curve).

Fig. 14 Measured photoelectron spectrum of fig.10 and the simulated one according to relation (7) (dashed curve).

Fig.15 Number of resolved photoelectron peaks for Quantacon (3 peaks) and HPMT (14 peaks).

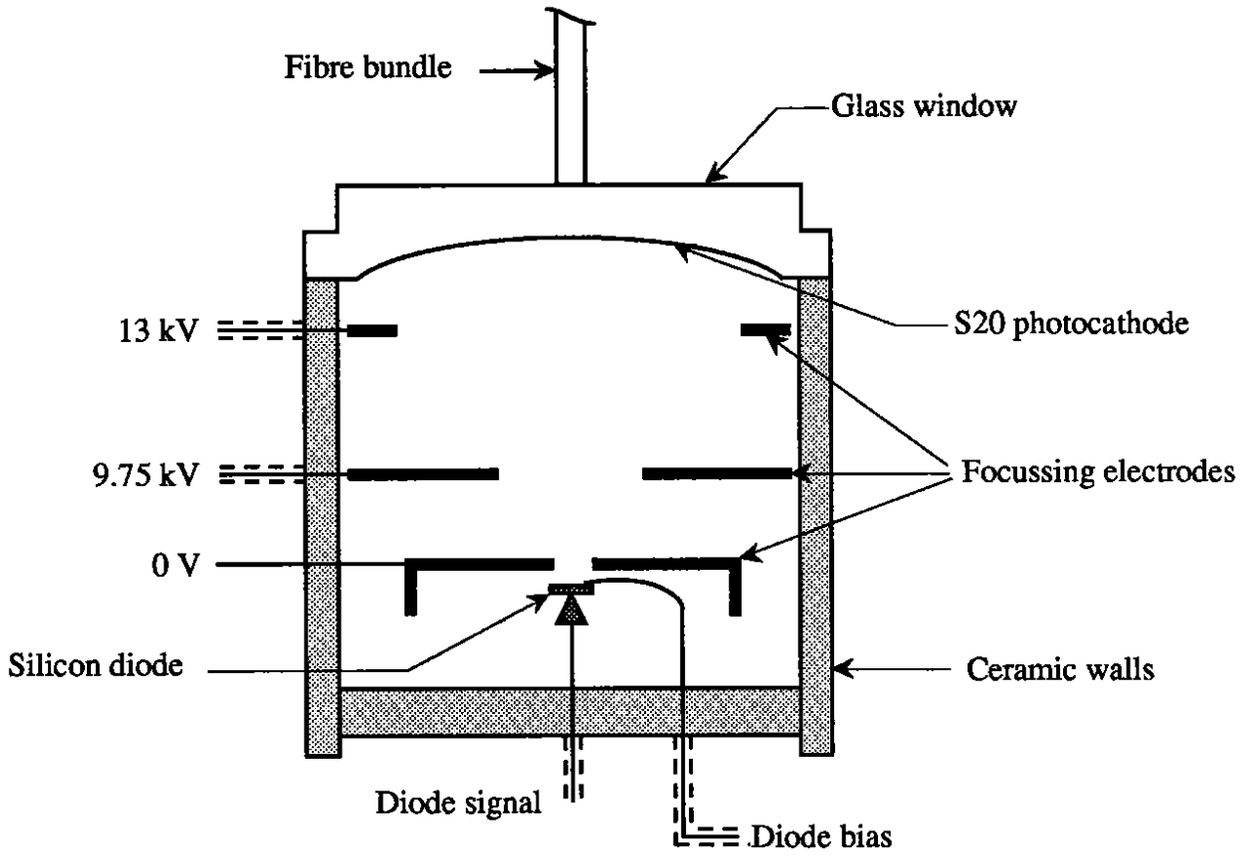
Fibre bundle
Glass window
13 kV
S20 photocathode
9.75 kV
Focussing electrodes
0 V
Silicon diode
Ceramic walls
Diode signal
Diode bias

Fig.1

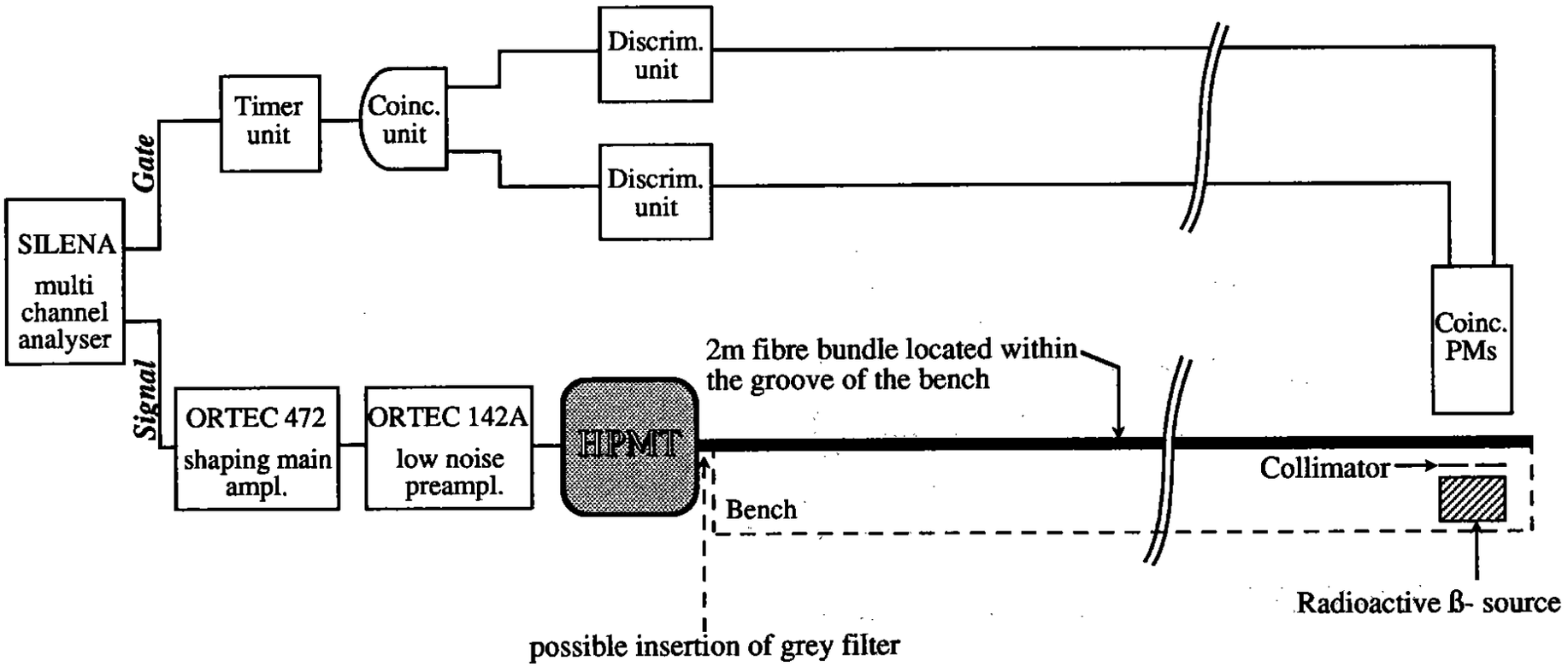
Discrim. unit
Timer unit
Coinc. unit
Discrim. unit
Gate
SILENA multi channel analyser
Coinc. PMs
2m fibre bundle located within the groove of the bench
Signal
ORTEC 472 shaping main ampl.
ORTEC 142A low noise preampl.
HPMT
Collimator
Bench
Radioactive ß- source
possible insertion of grey filter

Fig.2

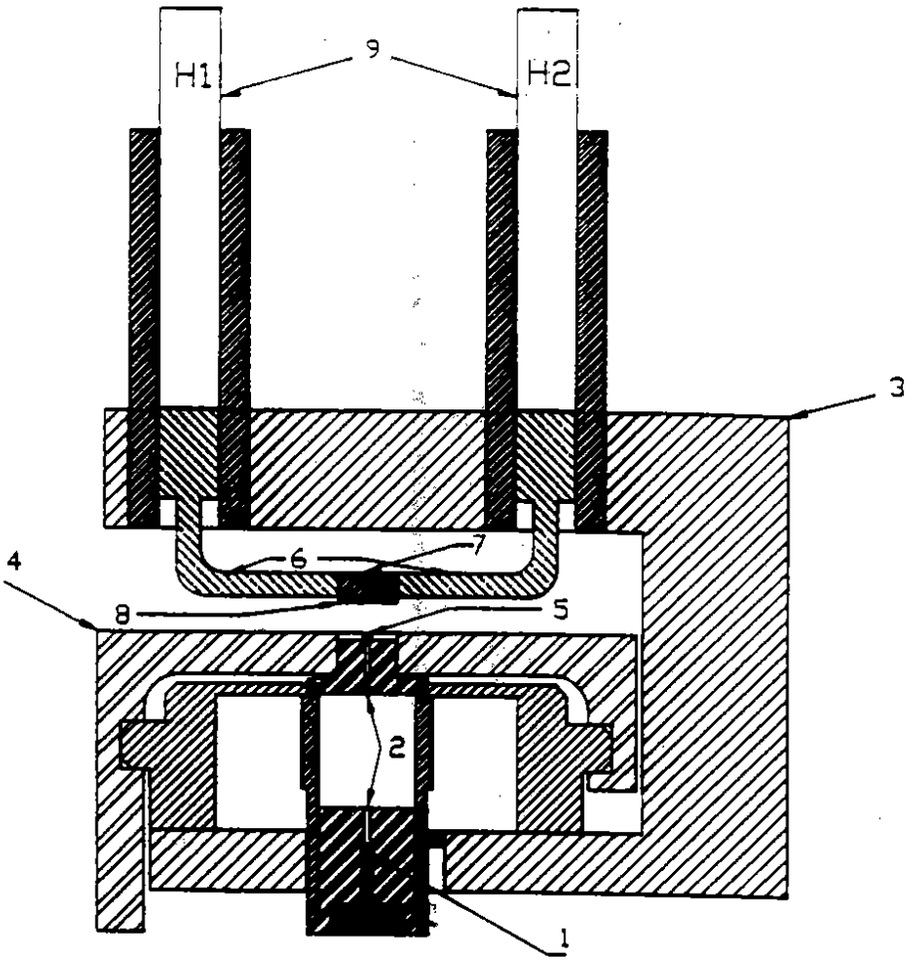

Fig.3

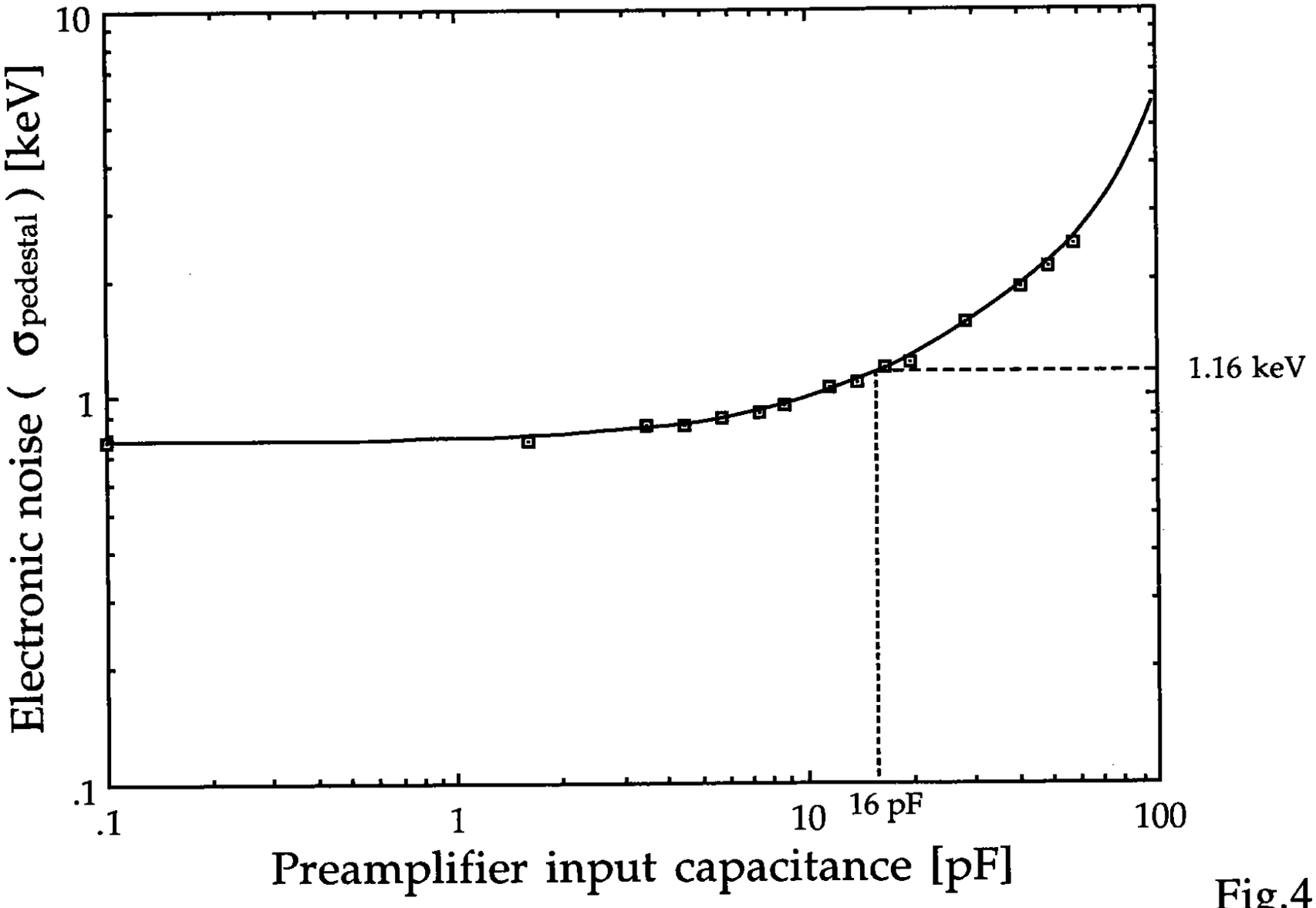
10
1
.1
Electronic noise (σpedestal) [keV]
1.16 keV
.1
1
10
16 pF
100
Preamplifier input capacitance [pF]

Fig.4

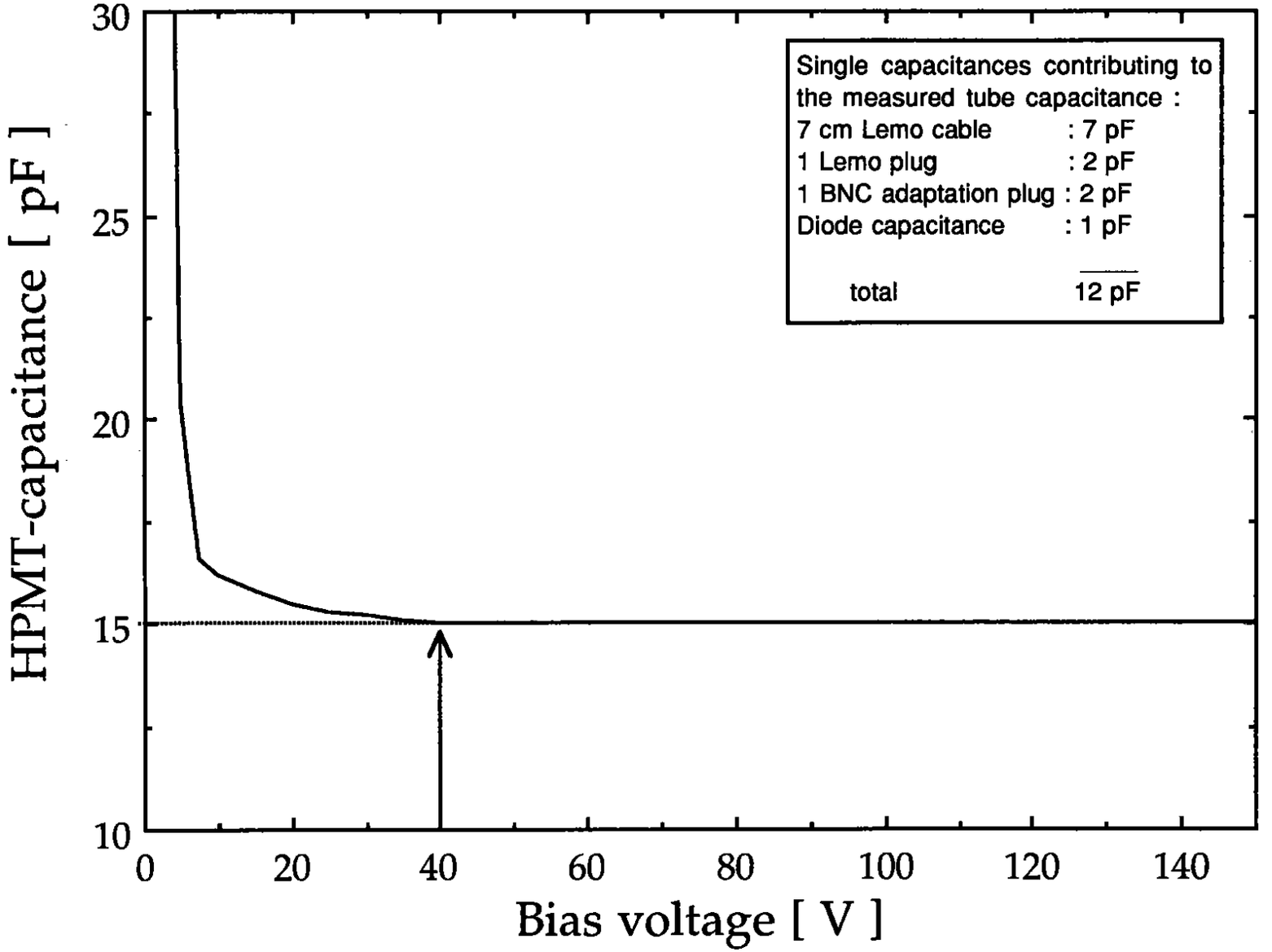
HPMT-capacitance [pF]
30
25
20
15
10
0
20
40
60
80
100
120
140
Bias voltage [V]
Single capacitances contributing to the measured tube capacitance :
7 cm Lemo cable : 7 pF
1 Lemo plug : 2 pF
1 BNC adaptation plug : 2 pF
Diode capacitance : 1 pF
total 12 pF

Fig.5

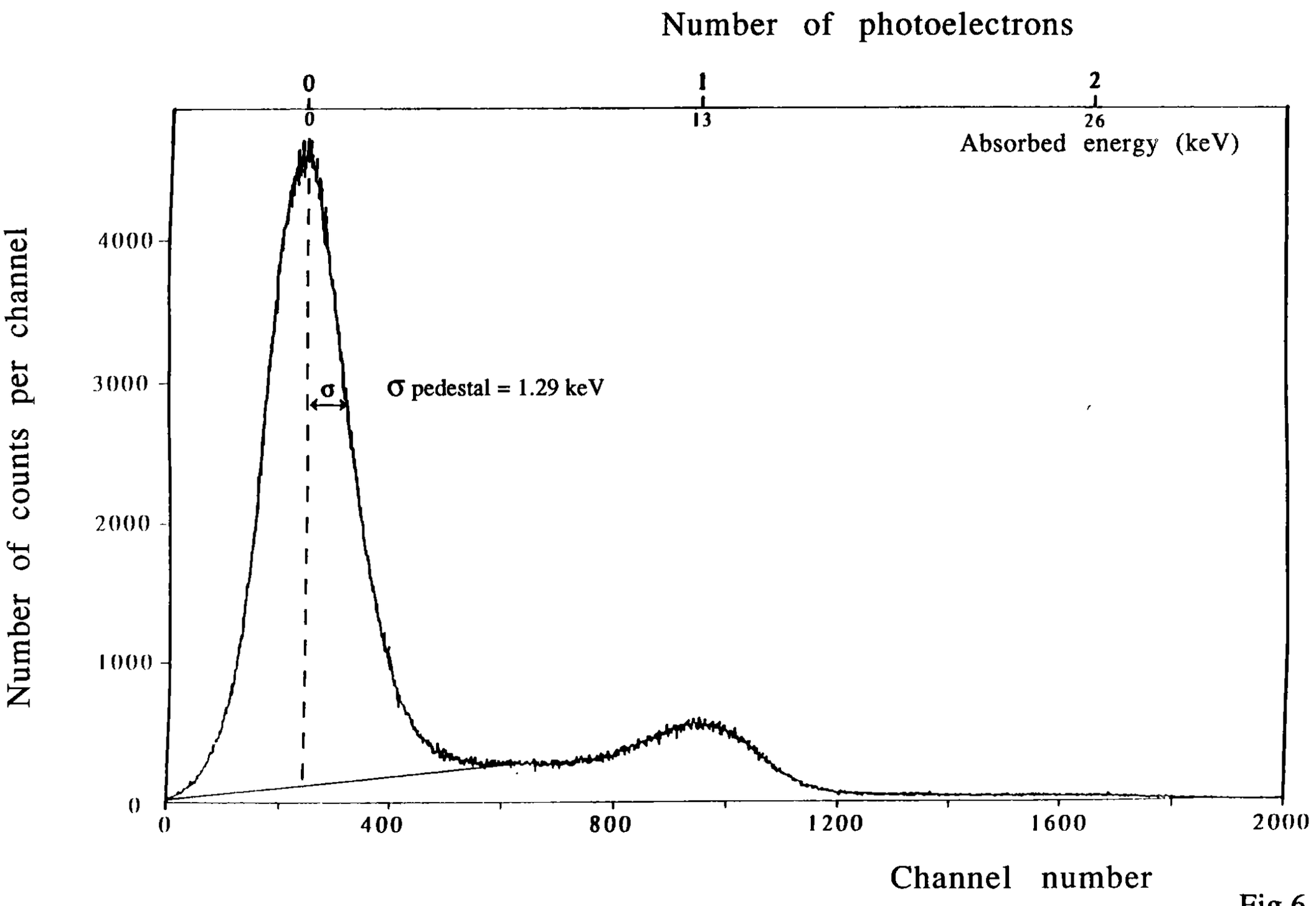
Number of photoelectrons
0
1
2
0
13
26
Absorbed energy (keV)
Number of counts per channel
4000
3000
2000
1000
0
σ
σ pedestal = 1.29 keV
0
400
800
1200
1600
2000
Channel number

Fig.6

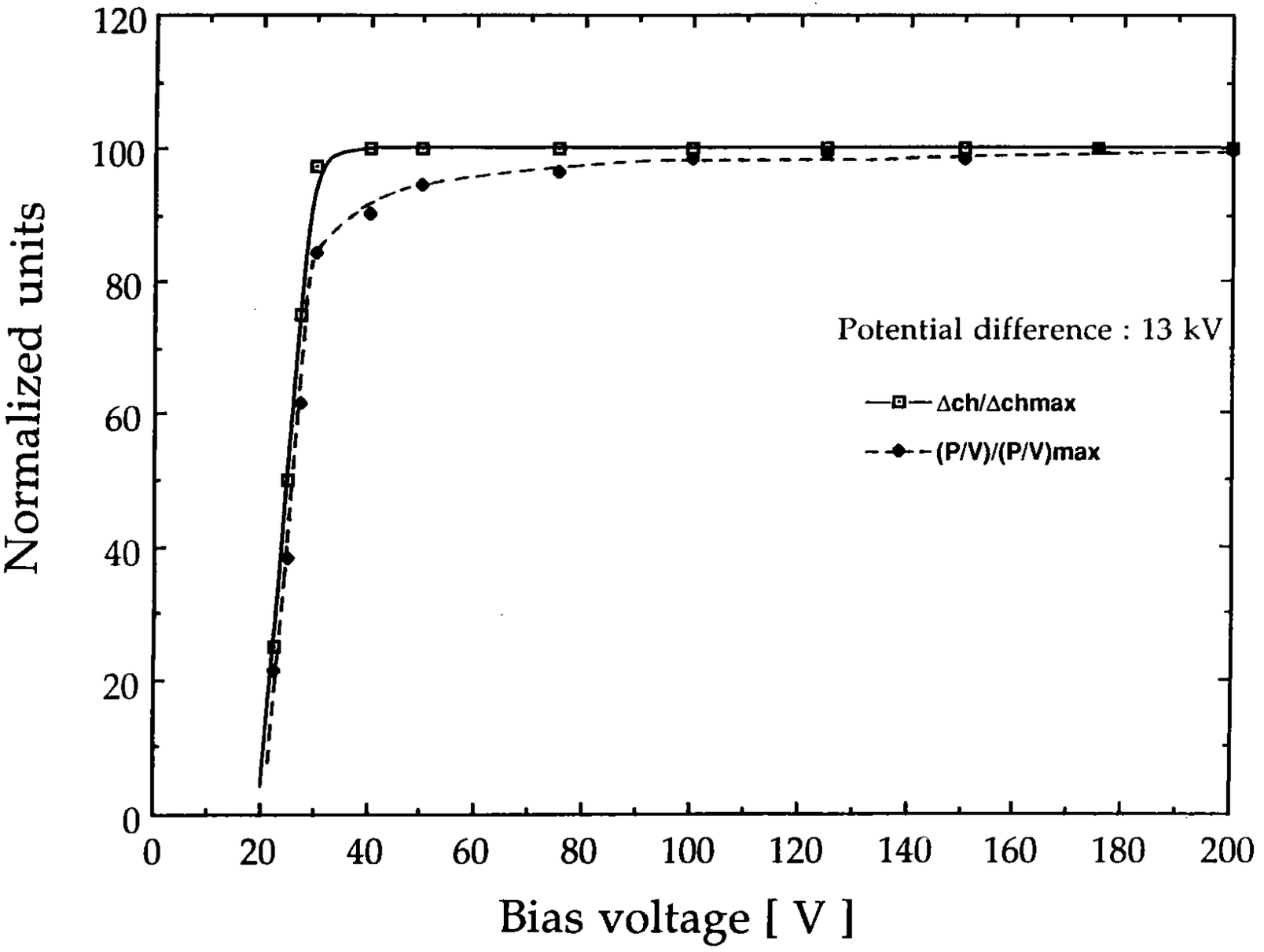
120
100
80
60
40
20
0
0
20
40
60
80
100
120
140
160
180
200
Normalized units
Bias voltage [V]
Potential difference : 13 kV
Δch/Δchmax
(P/V)/(P/V)max

Fig.7

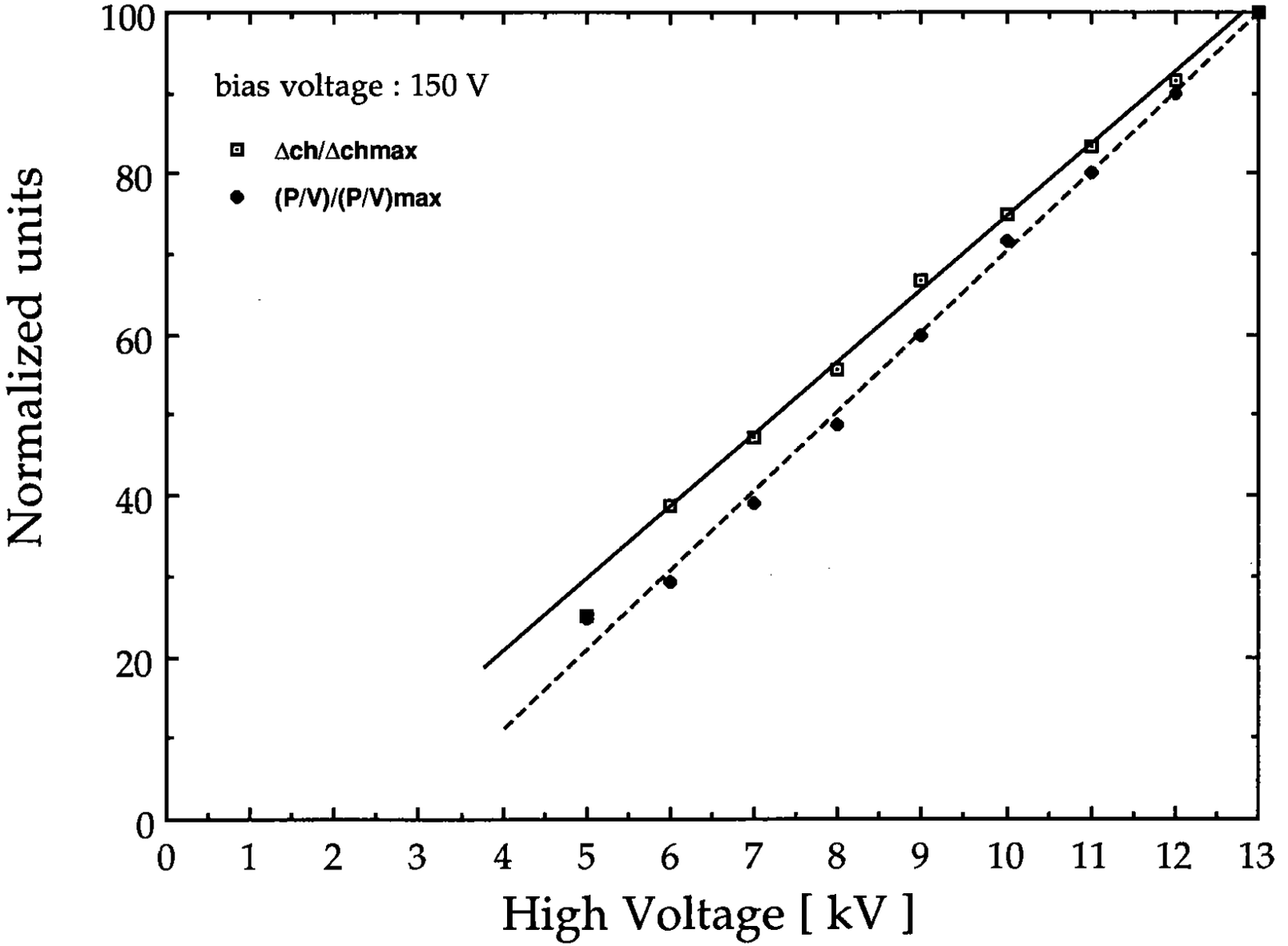
bias voltage : 150 V
Δch/Δchmax
(P/V)/(P/V)max
Normalized units
High Voltage [kV]
0
20
40
60
80
100
0
1
2
3
4
5
6
7
8
9
10
11
12
13

Fig.8

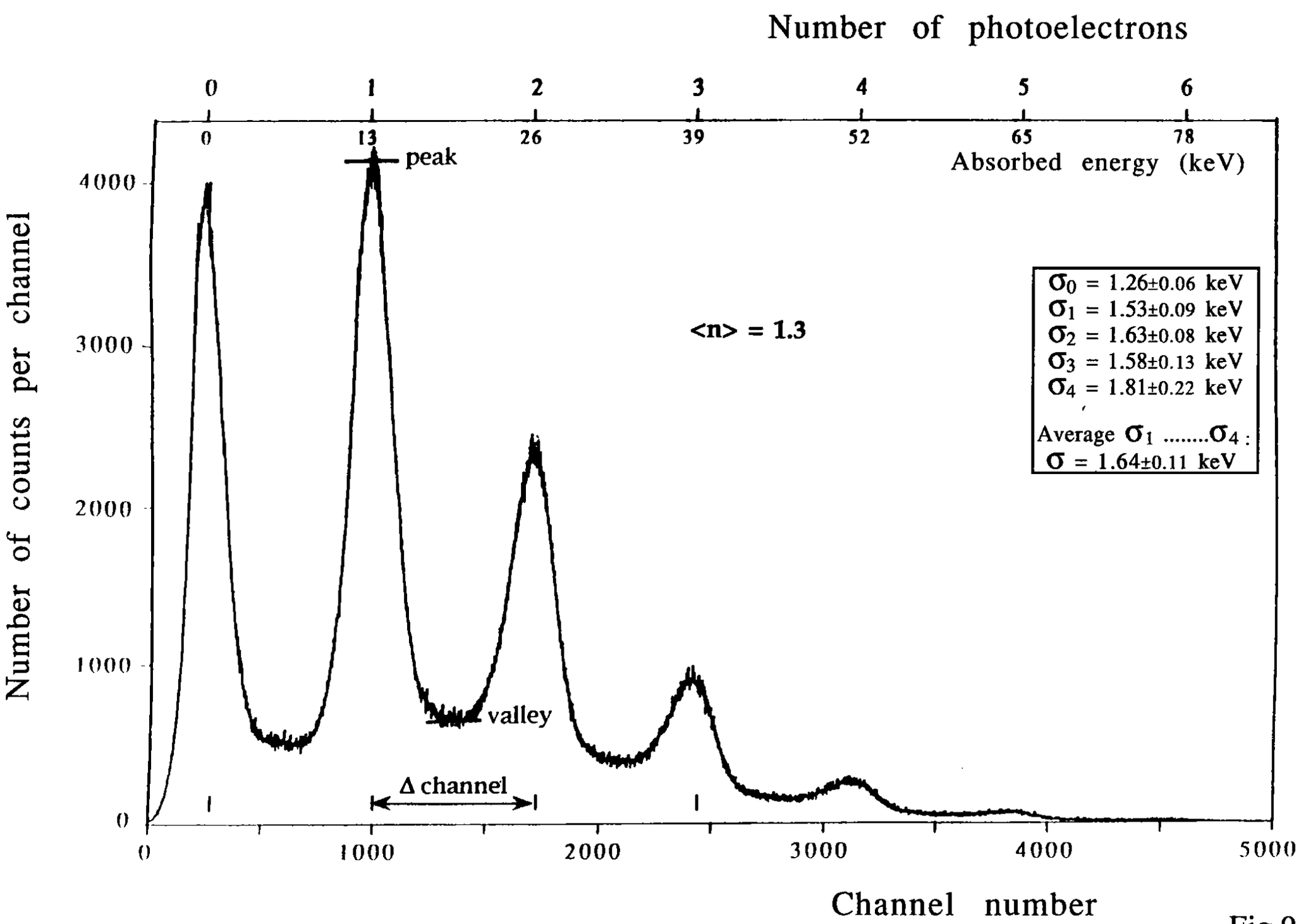
Number of photoelectrons
0
1
2
3
4
5
6
0
13
26
39
52
65
78
Absorbed energy (keV)
peak
valley
Δ channel
<n> = 1.3
σ0 = 1.26±0.06 keV
σ1 = 1.53±0.09 keV
σ2 = 1.63±0.08 keV
σ3 = 1.58±0.13 keV
σ4 = 1.81±0.22 keV
Average σ1 .....σ4 :
σ = 1.64±0.11 keV
Number of counts per channel
4000
3000
2000
1000
0
0
1000
2000
3000
4000
5000
Channel number

Fig.9

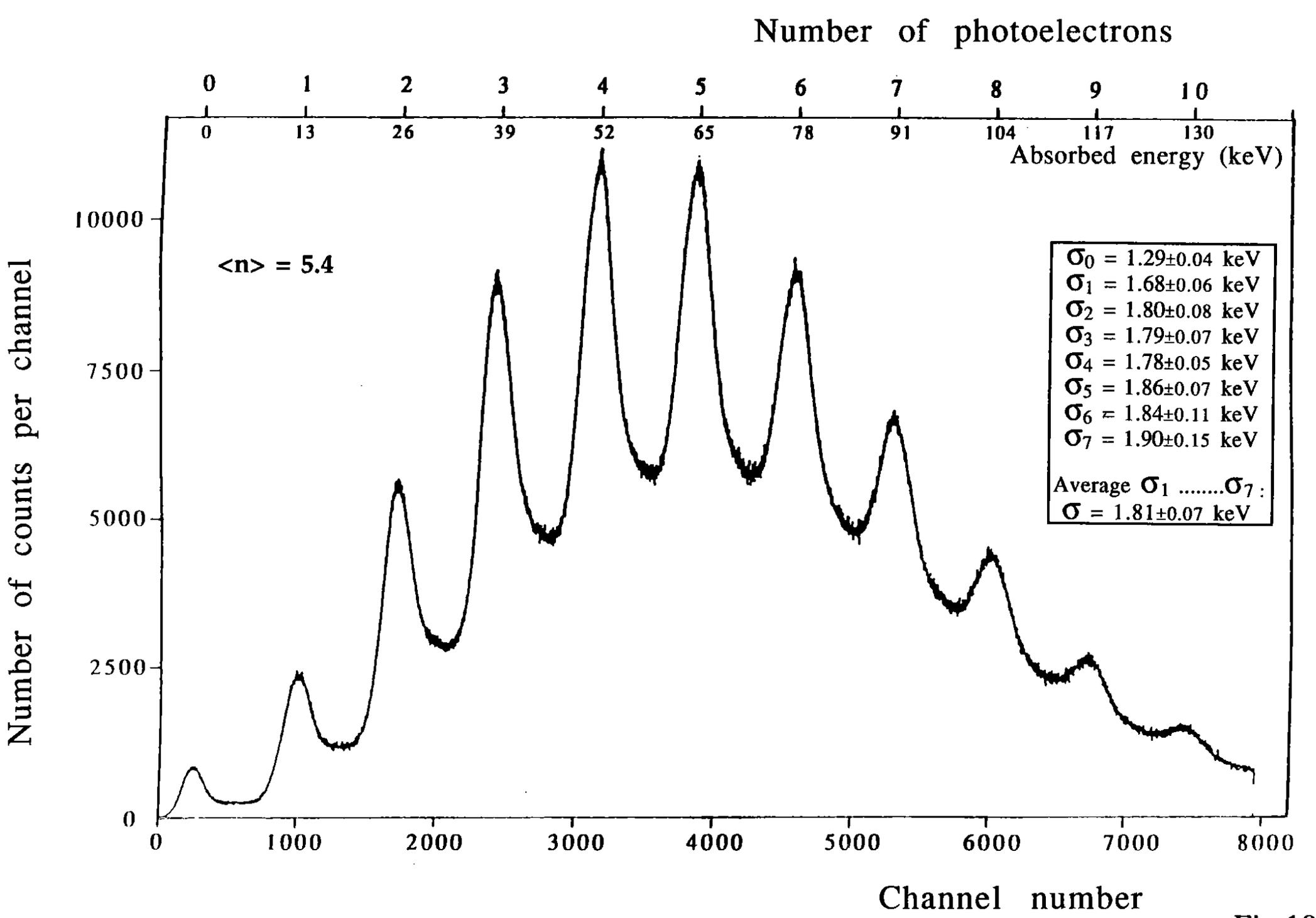
Number of photoelectrons
0 1 2 3 4 5 6 7 8 9 10
0 13 26 39 52 65 78 91 104 117 130
Absorbed energy (keV)
<n> = 5.4
σ0 = 1.29±0.04 keV
σ1 = 1.68±0.06 keV
σ2 = 1.80±0.08 keV
σ3 = 1.79±0.07 keV
σ4 = 1.78±0.05 keV
σ5 = 1.86±0.07 keV
σ6 = 1.84±0.11 keV
σ7 = 1.90±0.15 keV
Average σ1 .....σ7 :
σ = 1.81±0.07 keV
Number of counts per channel
10000
7500
5000
2500
0
0 1000 2000 3000 4000 5000 6000 7000 8000
Channel number

Fig.10

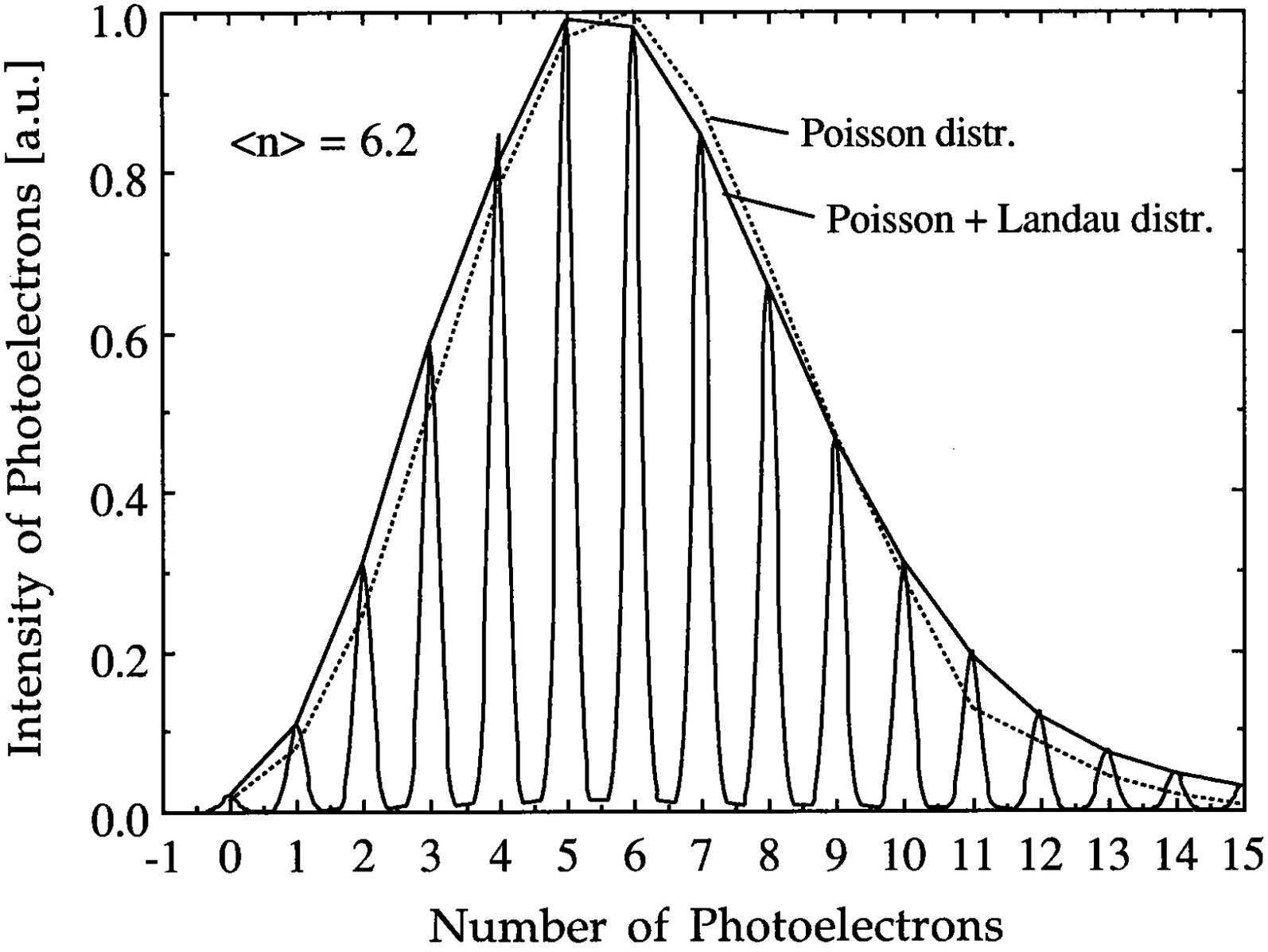
1.0
0.8
0.6
0.4
0.2
0.0
Intensity of Photoelectrons [a.u.]
<n> = 6.2
Poisson distr.
Poisson + Landau distr.
-1 0 1 2 3 4 5 6 7 8 9 10 11 12 13 14 15
Number of Photoelectrons

Fig.11

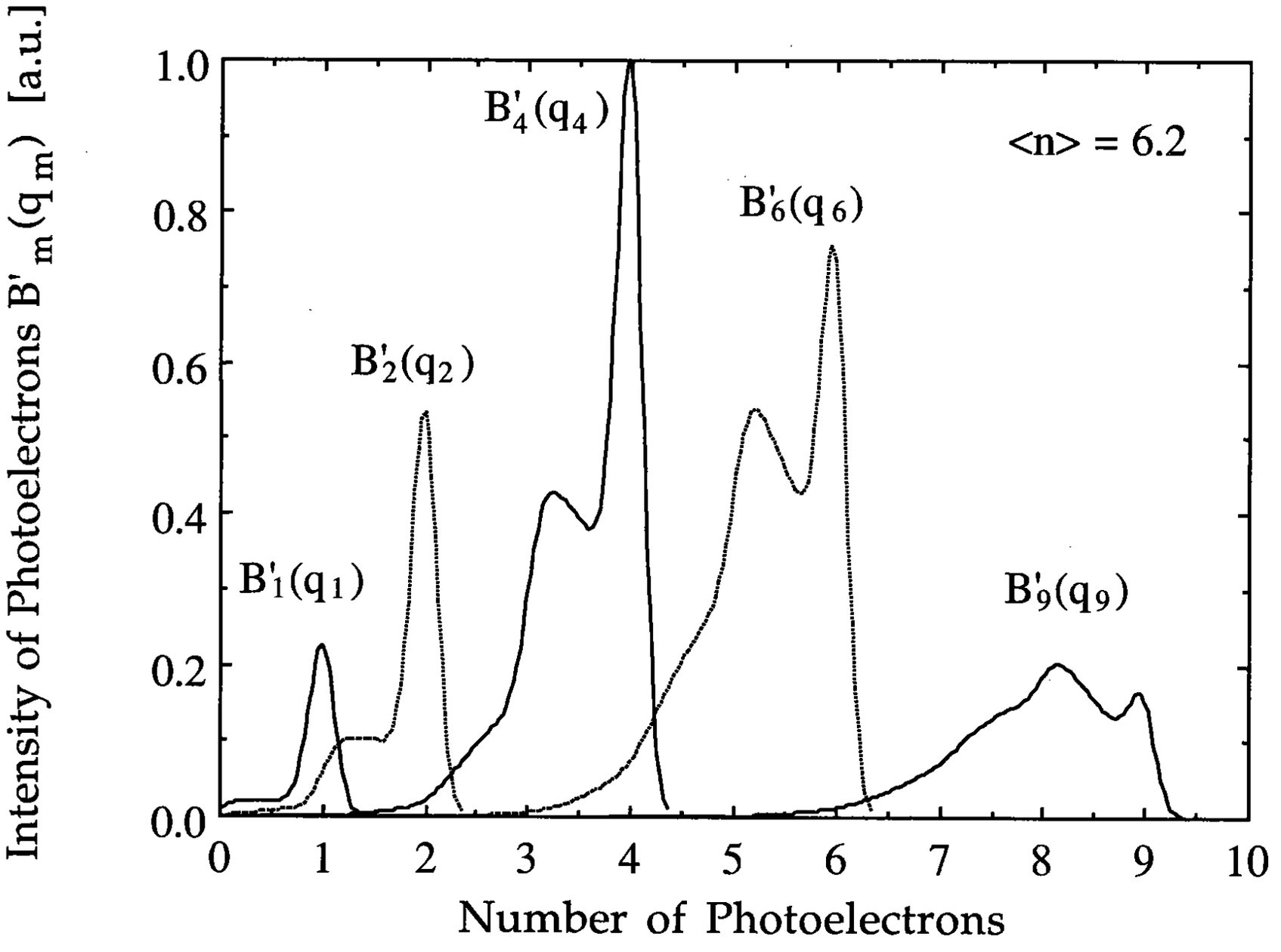
Intensity of Photoelectrons B'm(qm) [a.u.]
1.0
0.8
0.6
0.4
0.2
0.0
0
1
2
3
4
5
6
7
8
9
10
Number of Photoelectrons
B'1(q1)
B'2(q2)
B'4(q4)
B'6(q6)
B'9(q9)
<n> = 6.2

Fig.12

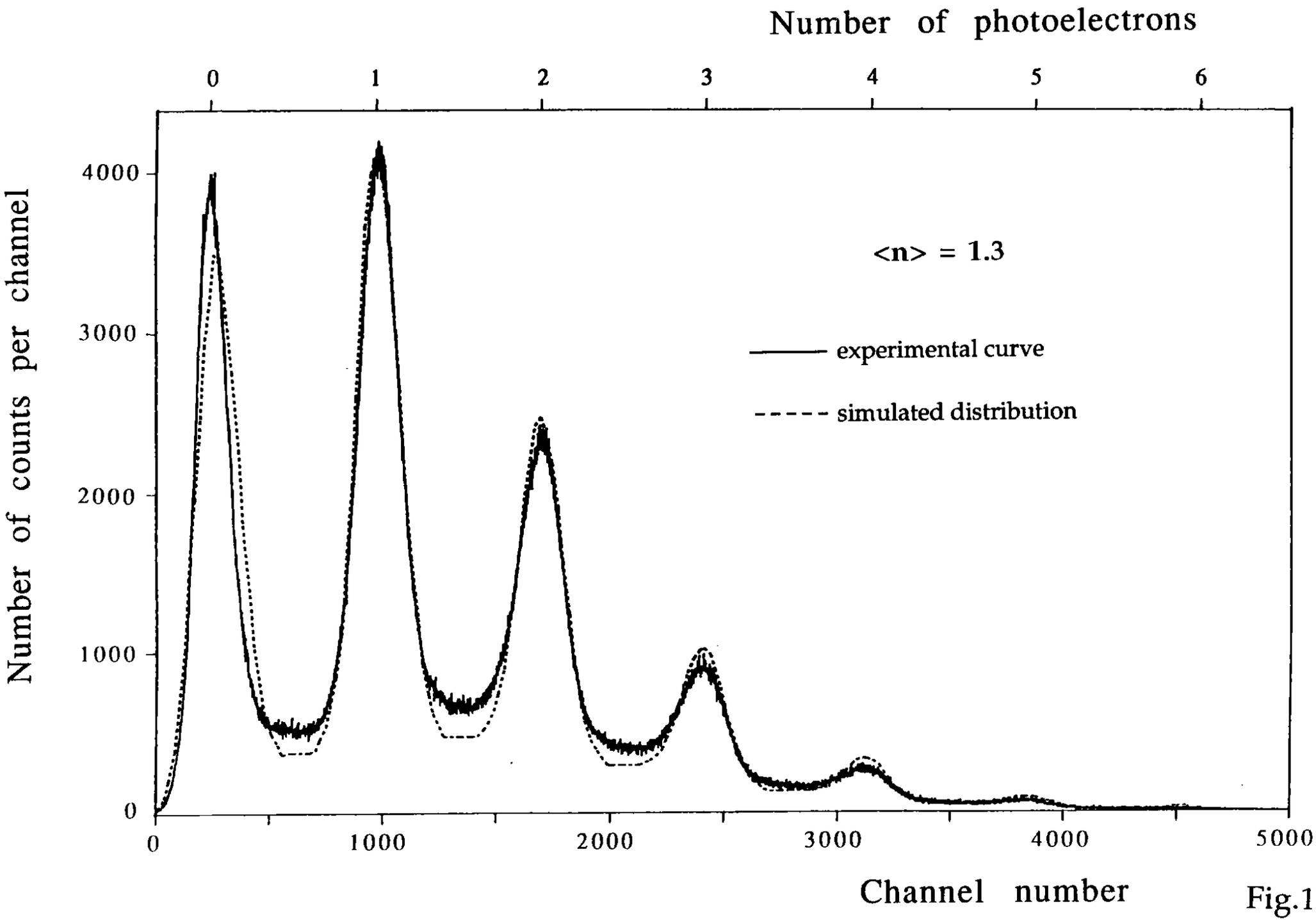
Number of photoelectrons
0
1
2
3
4
5
6
Number of counts per channel
4000
3000
2000
1000
0
<n> = 1.3
experimental curve
simulated distribution
0
1000
2000
3000
4000
5000
Channel number

Fig.13

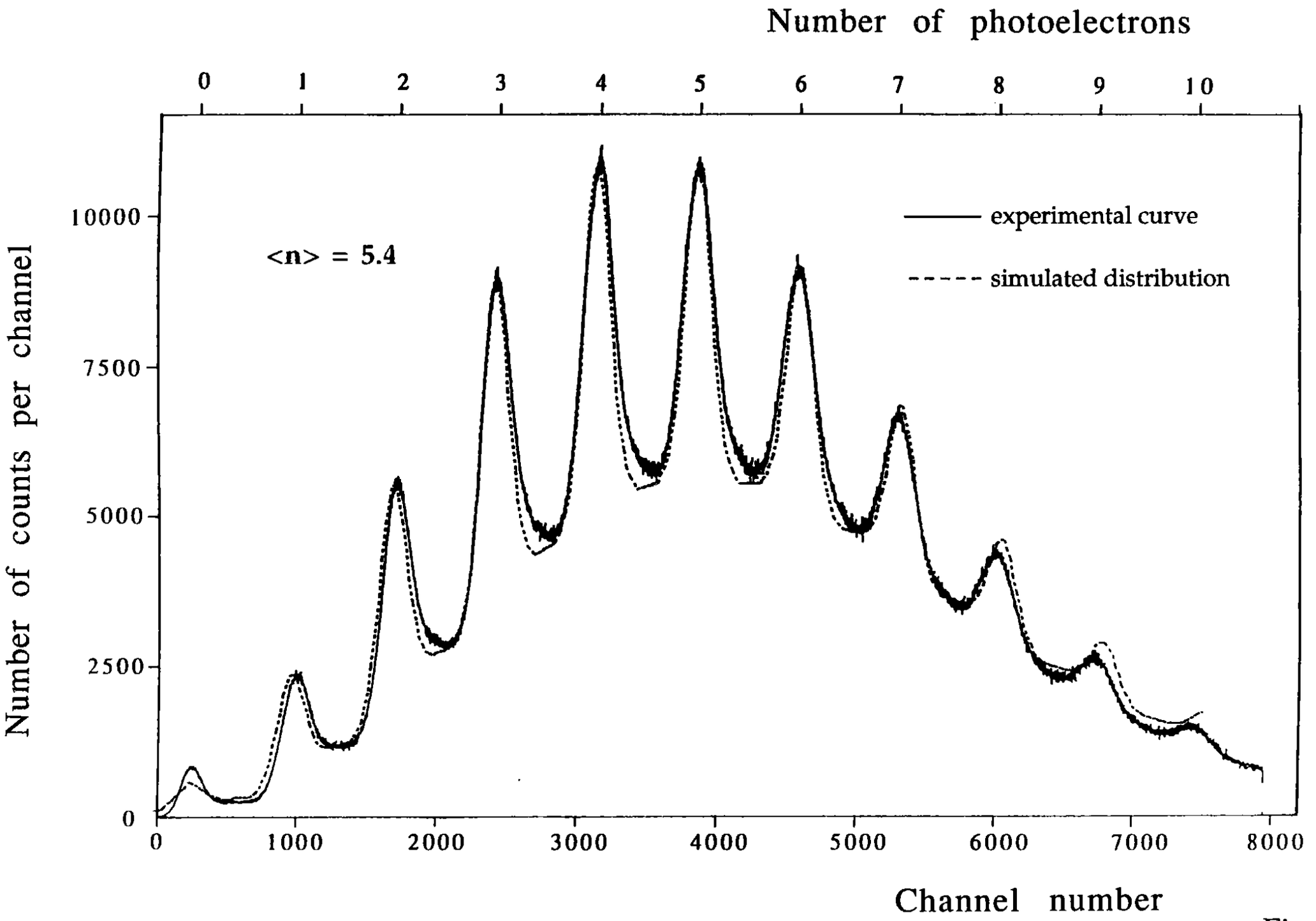
Number of photoelectrons
0
1
2
3
4
5
6
7
8
9
10
<n> = 5.4
experimental curve
simulated distribution
Number of counts per channel
10000
7500
5000
2500
0
0
1000
2000
3000
4000
5000
6000
7000
8000
Channel number

Fig.14

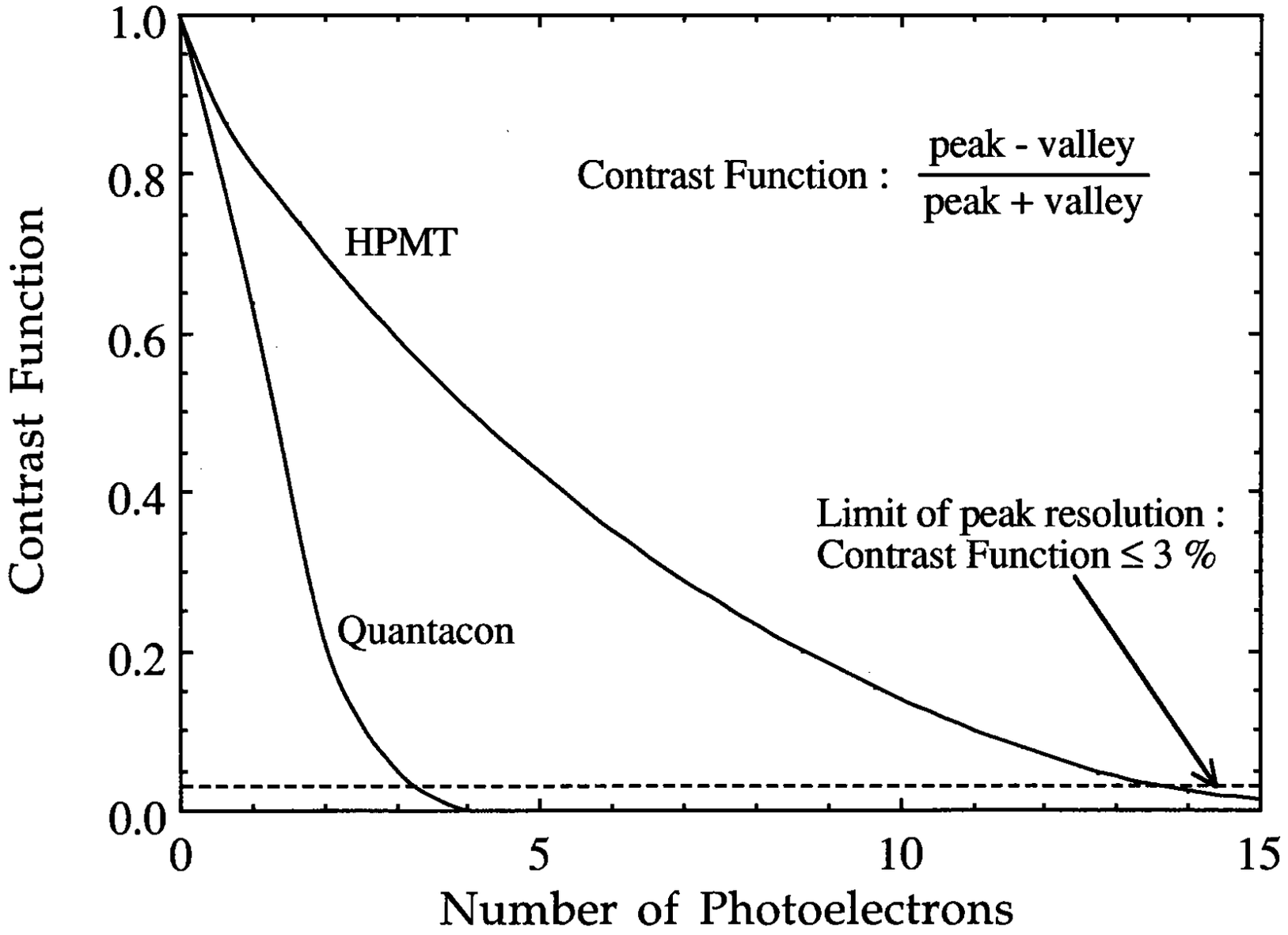
1.0
0.8
0.6
0.4
0.2
0.0
Contrast Function
0
5
10
15
Number of Photoelectrons
Contrast Function : peak - valley / peak + valley
HPMT
Quantacon
Limit of peak resolution :
Contrast Function ≤ 3 %

Fig.15